Experimental Evidence of Self-Localized and Propagating Spin Wave Modes in Obliquely Magnetized Current-Driven Nanocontacts

Stefano Bonetti,[1,*] Vasil Tiberkevich,[2] Giancarlo Consolo,[3,4] Giovanni Finocchio,[4] Pranaba Muduli,[5] Fred Mancoff,[6] Andrei Slavin,[2] and Johan Åkerman[1,5]

[1]*Materials Physics, Royal Institute of Technology, Electrum 229, 164 40 Kista, Sweden*
[2]*Department of Physics, Oakland University, Rochester, Michigan 48309, USA*
[3]*Department of Physics and CNISM, University of Ferrara, Ferrara, Italy*
[4]*Department of Matter Physics and Electronic Engineering, University of Messina, Messina, Italy*
[5]*Department of Physics, University of Gothenburg, Gothenburg, Sweden*
[6]*Everspin Technologies, Inc., 1300 N. Alma School Road, Chandler Arizona, USA*

(Received 17 September 2009; revised manuscript received 28 May 2010; published 17 November 2010)

Through detailed experimental studies of the angular dependence of spin wave excitations in nanocontact-based spin-torque oscillators, we demonstrate that two distinct spin wave modes can be excited, with different frequency, threshold currents, and frequency tunability. Using analytical theory and micromagnetic simulations we identify one mode as an exchange-dominated propagating spin wave, and the other as a self-localized nonlinear spin wave bullet. Wavelet-based analysis of the simulations indicates that the apparent simultaneous excitation of both modes results from rapid mode hopping induced by the Oersted field.

DOI: 10.1103/PhysRevLett.105.217204 PACS numbers: 75.30.Ds, 85.75.−d

Spin-polarized currents passing through a thin magnetic film can excite spin waves via the spin-transfer-torque effect [1,2]. In his pioneering paper [3], Slonczewski predicted that such spin waves, excited in a perpendicularly magnetized free layer underneath a nanocontact [4], would be exchange dominated, propagating radially from the nanocontact region, with a wave number k inversely proportional to the nanocontact radius R_c ($k \simeq 1.2/R_c$). Rippard *et al.* [5] subsequently demonstrated that, while Slonczewski's theory correctly describes the frequency and threshold current of spin waves excited in perpendicularly magnetized films, it fails to describe spin waves excited when the same film is magnetized in the plane. It was later shown theoretically that in the case of in-plane magnetization, apart from the Slonczewski-like propagating spin wave mode, it is possible to excite a self-localized nonlinear spin wave mode of solitonic character—a so-called standing spin wave bullet [6]. While the current-induced excitation of the spin wave bullet was subsequently confirmed in several numerical simulations [7–10], and angular dependent measurements have been presented in the literature [11], no clear experimental evidence on the nature of the modes excited by a spin-polarized current in a magnetic nanocontact has been presented yet.

In this Letter, we study the angular dependence of spin wave excitations in a nanocontact-based spin-torque oscillator (STO), and demonstrate that when the free layer is magnetized at sufficiently small angles $\theta_e \lesssim 55°$ with respect to the plane, two distinct and qualitatively different spin wave modes can be excited by the current passing through the nanocontact. The two modes have different frequencies f, different threshold currents I_{th}, and opposite signs of the frequency tunability df/dI. Through comparison with theory [6,12] and micromagnetic simulations, we show that the higher-frequency, blueshifted mode can be identified as the Slonczewski propagating mode, and that the lower-frequency, redshifting mode exhibits all the predicted properties of a localized spin wave bullet. Using time-frequency wavelet-based analysis of the results of our micromagnetic simulations, we also demonstrate that the apparent simultaneous excitation of both modes, as observed in our frequency domain experiments, results from the persistent switching (of sub-ns time scales) between the two modes caused by the spatially nonuniform Oersted field of the bias current.

The magnetically active part of the sample is a $Co_{81}Fe_{19}$(20 nm)/Cu(6 nm)/$Ni_{80}Fe_{20}$(4.5 nm) thin film trilayer, patterned into a 8 μm × 26 μm mesa. On top of this mesa, a circular Al nanocontact having nominal diameter $2R_c = 40$ nm was defined through SiO_2 using e-beam lithography (see Ref. [13] for details). An external magnetic field of constant magnitude ($\mu_0 H_e = 1.1$ T) was applied to the sample at an angle θ_e with respect to the film plane.

Details of the measurements setup are given in Ref. [14]. The excited spin waves modulate the magnetoresistance of the device and are detected as a microwave voltage signal. Microwave excitations were only observed for a single current polarity, corresponding to electrons flowing from the ''free'' (thin NiFe) to the ''fixed'' (thick CoFe) magnetic layer. All measurements were performed at room temperature. While the results presented here all come from a single sample, we have confirmed that the results obtained on several other devices are qualitatively similar.

Figure 1 shows the angular dependence of the microwave frequencies generated at a constant current of

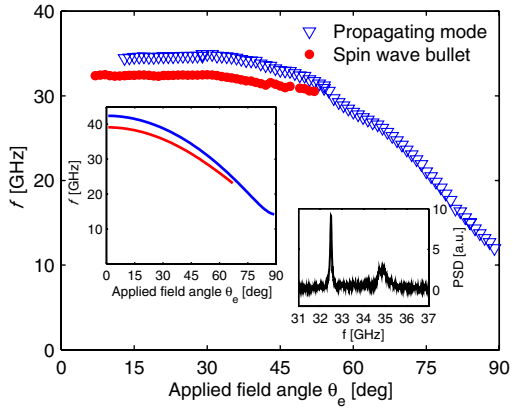

FIG. 1 (color online). Measured frequencies of the observed spin wave modes as a function of the applied field angle θ_e at $I = 14$ mA and $\mu_0 H_e = 1.1$ T. Left inset: theoretically calculated frequencies of the propagating (upper curve) and bullet (lower curve) modes at the current threshold, for nominal parameters of the nanocontact STO. Right inset: power spectrum at $\theta_e = 30$ deg, $I = 14$ mA.

$I = 14$ mA. The most striking feature is the existence of two distinct signals for sufficiently small values of θ_e. The frequencies of these two signals differ by about 2.5 GHz at angles up to $\theta_e = 40°$, and then start to approach each other up to a critical angle $\theta_e = \theta_{cr} \approx 55°$, where the lower-frequency signal disappears. The general behavior of the two signals remains the same at higher currents ($I =$ 18 mA), with a slight increase of both θ_{cr} and the frequency separation to about 58° and 3 GHz, respectively.

Figure 2 shows the angular dependence of the threshold current I_{th} for both signals. I_{th} is found using the method proposed in Refs. [15,16], and employed in Ref. [17]. We extracted I_{th} only for the magnetization angles $20° < \theta_e < 80°$, since outside this range the signal was too weak to allow for a reliable analysis. We note that the

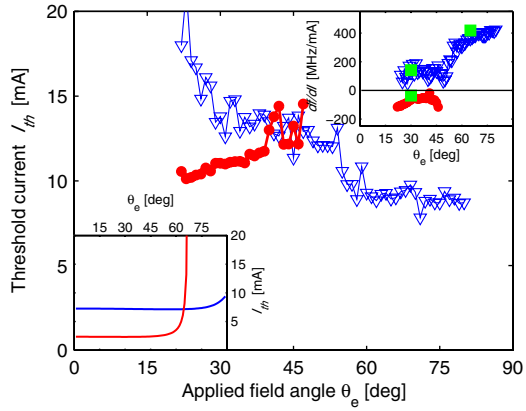

FIG. 2 (color online). Measured threshold current for the propagating (empty triangles) and bullet (filled circles) modes as a function of the applied field angle θ_e. Lower inset: theoretical threshold current vs applied field angle. Upper inset: df/dI vs θ_e for the propagating (empty triangles) and bullet (filled circles) modes as a function of θ_e. Filled squares are the results of micromagnetic simulations.

low-frequency signal always has the lower threshold current (within the noise of the analysis), in particular, at low field angles. As the angle increases, the I_{th} values for the two signals gradually approach each other and become essentially equal close to θ_{cr}. For the lower-frequency signal, the data are plotted up to $\theta_e = 47°$, since above this angle the signal is too low to allow for a reliable determination of I_{th}.

The upper inset in Fig. 2 shows the experimental tunabilities df/dI of the two signals, calculated as the slope of the linear fit of the f vs I characteristics in the interval $I - I_{th} = 3$ mA. Choosing this interval, we can estimate the above threshold tunability (i.e. intrinsic to spin-torque dynamics) excluding eventual "steps" in the dependence f vs I, such as the one occurring at $I \approx 14$ mA in Fig. 3(b). The lower-frequency signal always redshifts with the current ($df/dI < 0$), with values ranging from -40 to -110 MHz/mA. In contrast, the higher-frequency signal blueshifts with the current ($df/dI > 0$), with values ranging from $+50$ to $+150$ MHz/mA for $\theta_e < 45°$ and from $+300$ to $+400$ MHz/mA when $\theta_e > 55°$. The opposite tunability sign can be clearly seen in Figs. 3(a) and 3(b), where the microwave power of both signals is color mapped onto the frequency-current plane. At $\theta_e = 30°$ [Fig. 3(a)] both signals are visible, with a lower I_{th} and a clear redshift for the lower-frequency signal, and a higher I_{th} and a clear blueshift for the higher-frequency signal. At a larger magnetization angle, $\theta_e = 65°$ [Fig. 3(b)], only the higher-frequency, blueshifting signal is visible.

In order to gain a physical understanding of the experimental observations, we use the theoretical model of spin wave excitations developed in Refs. [6,12]. In this model, one of the excited modes is directly related to Slonczewski's propagating spin wave mode for a perpendicularly magnetized nanocontact STO [3], but it is now

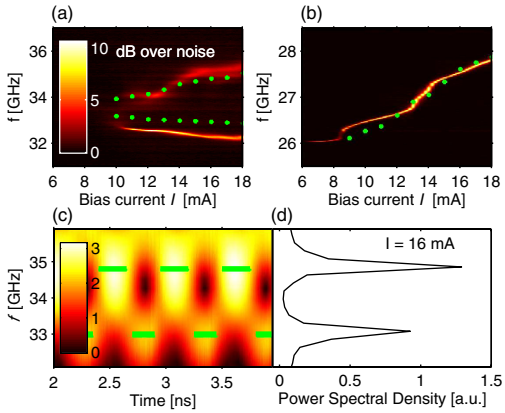

FIG. 3 (color online). Comparison of experiment with micromagnetic simulations: (a, b) Measured microwave power, presented as color maps onto the frequency-current plane, for two applied field angles, (a) $\theta_e = 30°$ and (b) $\theta_e = 65°$, where filled symbols show the results of the micromagnetic simulations. (c) Wavelet analysis (color scale in a.u.) and (d) fast Fourier transform of the micromagnetic simulation at $\theta_e = 30°$ and $I = 16$ mA.

generalized for the case of an oblique orientation of the free layer magnetization. The mode retains its propagating character; i.e., it carries energy away from the nanocontact area, and its threshold current is approximately given by

$$I_{\mathrm{th}}^{\mathrm{prop}} \approx [\Gamma(\theta_e) + 1.86D(\theta_e)/R_c^2]/\sigma(\theta_e), \quad (1)$$

where $\Gamma(\theta_e)$ is the Gilbert damping rate in the free layer, $D(\theta_e)$ is the spin wave dispersion coefficient, R_c is the nanocontact radius, and $\sigma(\theta_e)$ is the spin-polarization prefactor [see Eq. (2) in Ref. [6]]. The second term in Eq. (1) is independent of the spin wave damping Γ and describes radiative energy losses due to the propagating character of the mode. It is usually larger than the first term, which describes losses due to direct energy dissipation in the nanocontact area. The frequency of the propagating mode

$$\omega_{\mathrm{prop}} \approx \omega_0(\theta_e) + 1.44D(\theta_e)/R_c^2 + N(\theta_e)|a|^2 \quad (2)$$

is hence typically *higher* than the ferromagnetic resonance frequency ω_0 of the free layer and, depending on the sign of the nonlinear frequency shift, $N = \partial\omega/\partial|a_0|^2$, either blueshifts or redshifts with increasing current.

The model also predicts the existence of a self-localized nonlinear spin wave mode of a finite amplitude a_0. This spin wave "bullet" mode has a two-dimensional solitonic character and is stabilized by the competition between the natural positive magnetic damping and the negative damping caused by the spin-polarized current [6]. The expression for the threshold current of this nonpropagating mode lacks the radiative term, and, therefore, $I_{\mathrm{th}}^{\mathrm{bul}}$ is directly proportional to the spin wave damping:

$$I_{\mathrm{th}}^{\mathrm{bul}} \approx \beta\Gamma(\theta_e)/\sigma(\theta_e), \quad (3)$$

where the dimensionless coefficient $\beta \sim 1$ depends on the parameters of the system (for further details see [6]). As a consequence, the spin wave bullet mode for sufficiently small magnetization angles has a *lower* threshold current than the Slonczewski-like propagating mode.

The spin wave bullet mode exists only for the magnetization angles at which the nonlinearity is $N < 0$ and can counteract the dispersion-related spreading of the spin wave profile. Since N is a function of the magnetization angle, and changes sign from negative for an in-plane magnetization to positive for a perpendicular magnetization [16], the spin wave bullet mode only exists for applied field angles smaller than a certain critical value θ_{cr} [12]. As a direct consequence of the negative N, the frequency of the spin wave bullet mode

$$\omega_{\mathrm{bul}} \approx \omega_0(\theta_e) + N(\theta_e)|a_0|^2 \quad (4)$$

always lies *below* the ferromagnetic resonance frequency ω_0, and continues to *decrease* with increasing bias current.

The inset of Fig. 1 shows the calculated f vs θ_e for the two modes, using the nominal parameters of the experimental STO. The experimental data confirm the theoretical predictions, such as the existence of a critical angle below which a lower-frequency mode is excited, and a characteristic angular dependence of the mode frequencies. The inset of Fig. 2 shows the threshold curves I_{th} vs θ_e for both modes. Again, the experimental data demonstrate the same qualitative behavior as predicted by theory. In particular, I_{th} of the lower-frequency mode is always lower than that of the higher-frequency mode up to a critical angle $\theta_{\mathrm{cr}} \approx 65°$. The combined qualitative agreement provides a strong argument for identifying the observed higher-frequency mode as a propagating mode, and the lower-frequency mode as a spin wave bullet.

There are, however, some notable differences between the theory and our experiments, the most striking being the apparent *simultaneous* excitation of both modes. Such a coexcitation is neither supported by the theory [6,12], nor by micromagnetic simulations [7,9], where, in contrast, a hysteresis between the two modes was observed. Another significant difference is the lack of any observed redshift of the propagating mode. While our experiments clearly demonstrate that the propagating mode is blueshifted at all field angles, Eq. (2) predicts a red frequency shift for this mode when $N < 0$, i.e., for $\theta_e < \theta_{\mathrm{cr}}$, in clear contradiction with our experimental data. As we show below, both these effects can be explained by taking into account the large Oersted field generated by the bias current flowing through the nanocontact, which was ignored in [6,7,9,12], but can be accounted for in micromagnetic simulations.

Micromagnetic simulations were carried out in a box-shaped free layer volume $800 \times 800 \times 4.5$ nm^3 with constant cell size $4 \times 4 \times 4.5$ nm^3. A uniform spin-polarized current acted on a quasicylindrical subvolume of the free layer with an adjustable radius R_c. The material properties of the NiFe free layer were as follows: saturation magnetization $\mu_0 M_{S,\mathrm{free}} = 0.7$ T, the Gilbert damping constant $\alpha_G = 0.01$, the exchange constant $A = 1.1 \times 10^{-11}$ J/m, and the spin-torque efficiency $\epsilon = 0.3$. The thickness and saturation magnetization of the CoFe fixed layer were 20 nm and $\mu_0 M_{S,\mathrm{fixed}} = 1.8$ T, respectively, and a minimization of the fixed layer magnetostatic energy in the applied field determined the fixed layer magnetization angle and, consequently, the polarization angle of the spin-polarized current. No magneto-crystalline anisotropy, RKKY interaction, or dipolar coupling between the two magnetic layers were taken into account. The external field magnitude was fixed at $\mu_0 H_{\mathrm{ext}} = 1.15$ T, and its direction was varied to fit the experimental data. All simulations were done at $T = 0$ K.

To achieve the quantitative agreement between the experimental results (see Fig. 3) in our micromagnetic simulations [shown as symbols in Figs. 3(a) and 3(b)] we had to use the effective contact of radius $R_c = 32$ nm (instead of the nominal value of 20 nm) and shift the effective magnetization angles by 5° (35° and 70° instead of the nominal 30° and 65°). With these adjustments the quantitative agreement with the experimental data is remarkable: the excitation frequency, the range of the mode existence, and the frequency tunability of both the observed modes are well reproduced by the simulations. The effective contact radius is larger than nominal because of the following two effects:

(i) current crowding at the contact perimeter, essentially increasing the effective contact radius compared to a uniform current, and (ii) lateral current spread in the free and fixed layers. The difference in the values of the magnetization angles (10%) is within the experimental accuracy.

It is clear from our simulations that the inclusion of the current-induced Oersted field qualitatively changes the simulated magnetization dynamics. First, the Oersted field changes the sign of the derivative df/dI for the propagating mode, making it positive at all the investigated field angles. This effectively resolves the apparent discrepancy between our experimental observations and the analytic theory [6,12]. On the other hand, the same derivative df/dI for the bullet mode remains largely unchanged with the inclusion of the Oersted field. If we now add the simulated df/dI at 35° and 70° to the upper inset of Fig. 2, we find a remarkable *quantitative* agreement with the experimental values for both modes.

Second, the inclusion of the Oersted field also makes the simulations reproduce the apparent simultaneous excitation of the two spin wave modes. While our experimental setup is limited to measurements in the frequency domain, our micromagnetic simulations allow us to investigate the detailed temporal evolution of the instantaneous power in each mode. Figure 3(c) shows the result of a wavelet analysis [18] of the micromagnetic data, where the horizontal line segments indicate the frequency positions of the instantaneous power maxima at different time slots. Figure 3(d) shows the power spectral density corresponding to Fig. 3(c) and demonstrating the coexistence of two modes with different frequencies. Although these modes seem to coexist in the frequency domain [see Fig. 3(d)], the wavelet analysis [Fig. 3(c)] makes it clear that the two modes are never excited at the same time. The calculated instantaneous microwave power exhibits a persistent (at $T = 0$ K, also periodic) hopping between the two modes, with a very high hopping frequency exceeding 1.5 GHz. It is noteworthy that we only observe such hopping when the Oersted field is properly included, which is likely related to the strong spatial inhomogeneities it induces in the vicinity of the nanocontact [19,20]. Finally, the influence of the Oersted field also explains the large quantitative discrepancy between the analytically calculated I_{th} and the experimental value (Fig. 2). Previous micromagnetic simulations have demonstrated that the Oersted field can cause a substantial (up to fourfold) increase of I_{th} (see Fig. 2 in Ref. [20]), which hence agrees much better with our experimental data.

In conclusion, we have presented a detailed experimental study of the field angle dependence of spin wave excitations in nanocontact-based spin-torque oscillators. We find that two distinct and qualitatively very different spin wave modes can be excited for applied field angles $\theta_e \lesssim 55°$. Through a comparison of our experimental measurements of the three fundamental oscillation properties (f, df/dI, and I_{th}) with both previously developed analytic theories [3,6,12] and our own micromagnetic simulations, we unambiguously identify the higher-frequency mode as an exchange-dominated propagating spin wave, and the lower-frequency mode as a self-localized nonpropagating spin wave bullet. Our micromagnetic simulations also show that the Oersted field induced by the current flow is responsible for the rapid (sub-ns) hopping between the two modes, which in the frequency domain make them appear as being excited simultaneously.

We gratefully acknowledge financial support from The Swedish Foundation for Strategic Research (SSF), the Swedish Research Council (VR), the Göran Gustafsson Foundation, the Knut and Alice Wallenberg Foundation, the U.S. NSF (Grant No. ECCS-1001815), and the U.S. Army TARDEC, RDECOM (Contracts No. W56HZV-09-P-L564 and No. W56HZV-10-P-L687). J. Å. is a Royal Swedish Academy of Sciences Researcher supported by a grant from the Knut and Alice Wallenberg Foundation. Support from CNISM through Progetto Innesco (μ-BLS) is also acknowledged.

*bonetti@kth.se

[1] J. C. Slonczewski, J. Magn. Magn. Mater. **159**, L1 (1996).
[2] L. Berger, Phys. Rev. B **54**, 9353 (1996).
[3] J. C. Slonczewski, J. Magn. Magn. Mater. **195**, 261 (1999).
[4] M. Tsoi, A. G. M. Jansen, J. Bass, W.-C. Chiang, M. Seck, V. Tsoi, and P. Wyder, Phys. Rev. Lett. **80**, 4281 (1998).
[5] W. H. Rippard, M. R. Pufall, and T. J. Silva, Appl. Phys. Lett. **82**, 1260 (2003).
[6] A. Slavin and V. Tiberkevich, Phys. Rev. Lett. **95**, 237201 (2005).
[7] G. Consolo, B. Azzerboni, G. Gerhart, G. A. Melkov, V. Tiberkevich, and A. N. Slavin, Phys. Rev. B **76**, 144410 (2007).
[8] D. V. Berkov and N. L. Gorn, Phys. Rev. B **76**, 144414 (2007).
[9] G. Consolo, B. Azzerboni, L. Lopez-Diaz, G. Gerhart, E. Bankowski, V. Tiberkevich, and A. N. Slavin, Phys. Rev. B **78**, 014420 (2008).
[10] D. Berkov and J. Miltat, J. Magn. Magn. Mater. **320**, 1238 (2008).
[11] W. H. Rippard, M. R. Pufall, S. Kaka, T. J. Silva, and S. E. Russek, Phys. Rev. B **70**, 100406(R) (2004).
[12] G. Gerhart, E. Bankowski, G. A. Melkov, V. S. Tiberkevich, and A. N. Slavin, Phys. Rev. B **76**, 024437 (2007).
[13] F. B. Mancoff, N. D. Rizzo, B. N. Engel, and S. Tehrani, Appl. Phys. Lett. **88**, 112507 (2006).
[14] S. Bonetti, P. Muduli, F. Mancoff, and J. Åkerman, Appl. Phys. Lett. **94**, 102507 (2009).
[15] V. Tiberkevich, A. Slavin, and J.-V. Kim, Appl. Phys. Lett. **91**, 192506 (2007).
[16] A. Slavin and V. Tiberkevich, IEEE Trans. Magn. **45**, 1875 (2009).
[17] K. Kudo, T. Nagasawa, R. Sato, and K. Mizushima, J. Appl. Phys. **105**, 07D105 (2009).
[18] G. Siracusano, G. Finocchio, A. La Corte, G. Consolo, L. Torres, and B. Azzerboni, Phys. Rev. B **79**, 104438 (2009).
[19] G. Consolo, B. Azzerboni, G. Finocchio, L. Lopez-Diaz, and L. Torres, J. Appl. Phys. **101**, 09C108 (2007).
[20] G. Consolo, G. Finocchio, L. Lopez-Diaz, and B. Azzerboni, IEEE Trans. Magn. **45**, 5220 (2009).